Monitoring cell endocytosis of liposomes by real-time electrical impedance spectroscopy

Caviglia, Claudia; Garbarino, Francesca; Canali, Chiara; Melander, Fredrik; Raiteri, Roberto; Ferrari, Giorgio; Sampietro, Marco; Heiskanen, Arto; Andresen, Thomas Lars; Zor, Kinga

Total number of authors:
11

Published in:
Analytical and Bioanalytical Chemistry

Link to article, DOI:
10.1007/s00216-020-02592-x

Publication date:
2020

Document Version
Peer reviewed version

Analytical and Bioanalytical Chemistry
https://doi.org/10.1007/s00216-020-02592-x

RESEARCH PAPER

Monitoring cell endocytosis of liposomes by real-time electrical impedance spectroscopy

Claudia Caviglia[1,2] · Francesca Garbarino[3] · Chiara Canali[1,4] · Fredrik Melander[3] · Roberto Raiteri[5] · Giorgio Ferrari[6] · Marco Sampietro[6] · Arto Heiskanen[1] · Thomas Lars Andresen[3] · Kinga Zór[7] · Jenny Emnéus[1]

Received: 15 December 2019 / Revised: 4 March 2020 / Accepted: 9 March 2020

Abstract

Evaluation and understanding the effect of drug delivery in in vitro systems is fundamental in drug discovery. We present an assay based on real-time electrical impedance spectroscopy (EIS) measurements that can be used to follow the internalisation and cytotoxic effect of a matrix metalloproteinase (MMP)–sensitive liposome formulation loaded with oxaliplatin (OxPt) on colorectal cancer cells. The EIS response identified two different cellular processes: (i) a negative peak in the cell index (CI) within the first 5 h, due to onset of liposome endocytosis, followed by (ii) a subsequent CI increase, due to the reattachment of cells until the onset of cytotoxicity with a decrease in CI. Free OxPt or OxPt-loaded Stealth liposomes did not show this two-stage EIS response; the latter can be due to the fact that Stealth cannot be cleaved by MMPs and thus is not taken up by the cells. Real-time bright-field imaging supported the EIS data, showing variations in cell adherence and cell morphology after exposure to the different liposome formulations. A drastic decrease in cell coverage as well as rounding up of cells during the first 5 h of exposure to OxPt-loaded (MMP)-sensitive liposome formulation is reflected by the first negative EIS response, which indicates the onset of liposome endocytosis.

Keywords Real-time monitoring · Electrical impedance spectroscopy · Cell morphology · Matrix metalloproteinase · Cytotoxicity · Liposome endocytosis

Published in the topical collection featuring *Female Role Models in Analytical Chemistry.*

Francesca Garbarino and Chiara Canali contributed equally to this work.

Electronic supplementary material The online version of this article (https://doi.org/10.1007/s00216-020-02592-x) contains supplementary material, which is available to authorized users.

✉ Claudia Caviglia
claudia.caviglia@gmail.com

✉ Kinga Zór
kinzo@dtu.dk

✉ Jenny Emnéus
jemn@dtu.dk

[1] Department of Biotechnology and Biomedicine, Technical University of Denmark, Produktionstorvet, Building 423, 2800 Kongens Lyngby, Denmark

[2] Present address: Radiometer Medical ApS, Åkandevej 21, 2700 Brønshøj, Denmark

[3] Department of Health Technology, Technical University of Denmark, Ørsteds Plads, Building 345C, 2800 Kongens Lyngby, Denmark

[4] Present address: Novo Nordisk, Novo Nordisk Allé 1, 2880 Bagsværd, Denmark

[5] Department of Informatics, Bioengineering, Robotics and System Engineering, University of Genova, Via All'Opera Pia, 11A, 16145 Genoa, Italy

[6] Department of Electronics, Information and Bioengineering, Polytechnic University of Milan, P.za Leonardo da Vinci, 32, 20133 Milan, Italy

[7] Center for Intelligent Drug Delivery and Sensing Using Microcontainers and Nanomechanics, Department of Health Technology, Technical University of Denmark, Ørsteds Plads, Building 344, 2800 Kongens Lyngby, Denmark

Introduction

Understanding the effect of drug delivery systems on cell adhesion and morphology, proliferation, metabolism, communication and death is fundamental for optimising and enhancing anticancer drug treatment [1–3]. Hence, in parallel with the development and screening of new drug candidates, drug combinations and targeted drug delivery systems (TDDSs), there is an increasing demand for smart methods to study dynamic cellular processes regulating cancer cells' behaviour, as well as their interactions with drugs and TDDSs [4–7]. There are several commonly used assays that are particularly relevant for drug screening and toxicity testing in preclinical studies [8]. Among these, the most common ones assess the cell number and viability through cytotoxicity testing and include the Alamar Blue assay, the MTS (3-(4,5-dimethylthiazol-2-yl)-5-(3-carboxymethoxyphen-yl)-2-(4-sulfophenyl)-2H-tetrazolium) assay, the neutral red uptake assay, the ATP assay and the lactate dehydrogenase assay [9, 10]. These assays are based on single end-point measurements, performed on individual cell populations without providing real-time insight of the biological event of interest and are labour-intensive, resource-consuming and invasive, as they require multiple additions of chemicals and labelling steps that may affect the cellular functions. The development of label-free and real-time monitoring technologies has therefore become increasingly attractive for implementation in cell biology and drug discovery [11–13]. Electrochemical impedance spectroscopy (EIS) is one such method, first introduced by Giaever and Keese in 1984 [14], for real-time monitoring cell adhesion and spreading and subsequently applied to follow motility [15], proliferation [16] and cytotoxicity [1, 17–20]. The unique feature of the EIS response is based on the insulating properties of cells that reside on an electrode surface where an increased coverage of cells leads to an increase in the measured impedance. When cells are exposed to cytotoxic compounds, the cell integrity and adhesion are compromised, which consequently causes a decrease in the impedance, allowing non-invasive, label-free real-time monitoring, each cell population functioning as its own control. Optical microscopy is another key tool in drug development [21] with several solutions for real-time optical imaging of live cells [22, 23].

We have previously shown that EIS can be used to dynamically follow in real time the delivery of chemotherapeutic drugs to different kinds of cancer cells when free or loaded into liposomes, following the subsequent cell death [17]. Here, the metalloproteinase (MMP)-specific TDDS was studied in more detail by investigating the uptake and exposure of MMP producing colorectal HT1080 cancer cells to the cancer drug oxaliplatin (OxPt), delivered free in solution or loaded into different liposome formulations, equipped with or without MPP-cleavable polyethylene glycol (PEG)–peptide groups. As visualised in Fig. 1, an OxPt-liposome that contain MPP-cleavable PEG-peptides can be transformed into a positively charged liposome by MPPs released by the HT1080 cells and then readily be engulfed by these cells via the mechanism of endocytosis. In this way, the OxPt inside liposomes can be specifically delivered to MPP-producing cells if they contain MPP-cleavable PEG-peptides. Here, we studied several different drug-liposome formulations, i.e. free OxPt, OxPt-loaded liposomes with PEG-peptide, OxPt-loaded de-PEGylated liposomes and OxPt-loaded liposomes without PEG-peptide (Stealth). When studying this process dynamically and in real time using EIS, the resulting spectra (presented as CI, see Eq. 1) revealed a characteristic negative dip after 5 h, only for the liposome formulation equipped with the MMP cleavable PEG-peptide or the already de-PEGylated liposome formulation, indicating that the negative peak could signify the point when endocytosis of the liposomes takes place. To elucidate if this was the case, the EIS spectra time points for the different free and OxPt-liposome formulations were compared with those obtained using time-lapse bright-field (BF) images under the exact same conditions.

Material and methods

Chemicals and reagents

Sodium hydroxide, potassium hydroxide, hydrogen peroxide, cell culture–tested phosphate-buffered saline (PBS), fetal bovine serum (FBS), sodium chloride, laminin from Engelbreth-Holm-Swarm murine sarcoma basement membrane and OxPt (trans−/−diaminocyclohexane oxalatoplatinum; L-OHP) were purchased from Sigma-Aldrich Corporation (St. Louis, MO,

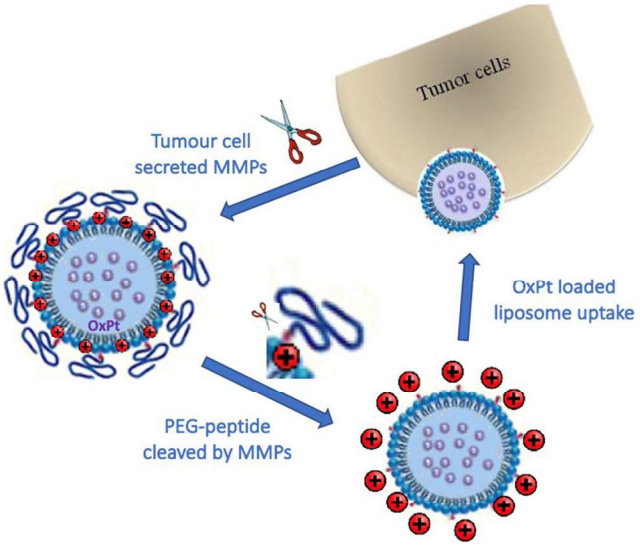

Fig. 1 Illustration of the endocytotic uptake of OxPt-loaded liposomes after cleavage of PEGylated peptide arms by MMPs (scissor) secreted by certain tumour cells, like colorectal HT1080 cells

USA). Dulbecco's Modified Eagle Medium (DMEM), Trypsin-EDTA (0.05%) and penicillin/streptomycin (P/S) were purchased from Life Technologies Ltd. (Paisley, UK). CellTiter 96® aqueous non-radioactive cell proliferation assay (MTS) was purchased from Promega Corporation (Madison, WI, USA). Thermolysin was purchased from Sigma-Aldrich Corporation (St. Louis, MO, USA). 1-Palmitoyl-2-oleoyl-sn-glycero-3-phosphocholine (POPC), 1,2-distearoyl-sn-glycero-3-phosphocholine (DSPC), 1,2-dioleoyl-3-trimethylammonium-propane (DOTAP) 1,2-distearoyl-*sn*-glycero-3-phosphoethanolamine-N-[amino(polyethylene glycol)-2000] (DSPE-PEG2000) and cholesterol were from Avanti Polar lipids, Inc. (Alabaster, AL, USA).

Preparation of liposomes

Liposomes were prepared by dissolving lipids in *tert*-butanol/water (9/1) solution followed by freeze drying. The following molar ratios were used: MMP-sensitive PEGylated liposomes (PEG-Lipo-OxPt):POPC/cholesterol/DOTAP/Cleavable-PEG:55/32/5/8, Stealth liposomes (Stealth):DSPC/cholesterol/DSPE-PEG2000:55/40/5. The freeze-dried lipid powder was hydrated in OxPt-solution (15 mg/ml, 10 mM Hepes and 5% glucose, pH 7.4) for 1 h at 65 °C while stirring and vortexing. The resulting vesicles were extruded with a high-pressure extruder (Northern lipids Inc. Burnaby, Canada) by passing the liposomes two times through two stacked 200 nm polycarbonate filter (Whatman, Maidstone, UK) followed by five passes through two 100 nm filters. The temperature was maintained at 65 °C during the extrusion process. Free OxPt was removed by dialysis using a dialysis cassette (Slide-A-Lyzer, 10 000 MWCO, Pierce, Fischer Scientific, Slangerup, Denmark) against 100× volumes of 10 mM Hepes and 5% glucose, pH 7.4 with three buffer changes. Encapsulated OxPt and phospholipid content were measured by ICP-MS (ICAPq, Thermo Scientific, Hvidovre, Denmark). Spin-filtration (Amicon ultra, 100K, Merck Life Science, Denmark) was used to measure the degree of encapsulation and ensure that less than 1% of OxPt was present on the outside of the liposomes. The particle size and charge were determined with a Zetasizer (Brookhaven Instruments Ltd., NY, USA).

De-PEGylated OxPt-loaded liposomes (De-PEG-Lipo-OxPt) were obtained through digestion with protease (thermolysin), 20 µl of liposomes were mixed with 180 µl of HEPES-buffered saline (NaCl (100 mm), HEPES (50 mM pH 7.4), $CaCl_2$ (1 mM) and $ZnCl_2$ (2 µM) supplemented with thermolysin (20 µg/ml)). The cleavage was performed overnight at 37 °C.

Cell culture

HT1080 cells (cat. No. 85060701) were purchased from Sigma-Aldrich Corporation (St. Louis, MO, USA). In preparation for experiments, cells were cultured in standard T25 flasks with regular medium exchange every 2 days. Prior to seeding cells, as previously described by Caviglia et al. [18], on microelectrode chips for monitoring EIS, cell suspensions were prepared by standard trypsinisation using a Trypsin-EDTA solution. Cells were centrifuged for 5 min at 900 rpm and 20 °C followed by resuspension in cell culture medium. The cell number was determined using a standard haemocytometer and the desired cell densities were prepared by diluting the initial cell suspension with fresh culture medium.

Prior to seeding cells in the cell culture well for EIS-based monitoring, each microelectrode chip was cleaned following a previously described method by L. M. Fischer et al. [24] which includes a chemical (10 min in the mixture of 25% H_2O_2/50 mM KOH) and an electrochemical (potential sweep in 50 mM KOH between −200 and −1200 mV) step. Sterilisation of the culture well was performed by a 20-min treatment with 500 mM NaOH followed by thorough rinsing with PBS as demonstrated previously [4]. To promote cell adhesion, the chip surface was modified using laminin (20 µg/ml; 2 h, 37 °C). The applied cleaning procedure facilitated the reusability of the microelectrode chips. Each chip was used for three experiments.

All cell preparations were kept in an ordinary humidified incubator at 37 °C in an atmosphere of 5% CO_2 in the air. HT1080 cells were cultured in DMEM supplemented with 10% FBS and 1% penicillin/streptomycin.

Instrumentation and experimental setup for real-time EIS analysis

The impedance measurement setup is composed of a plastic cell culture unit having a microelectrode chip with an array of 12 interdigitated electrodes (IDE), fabricated based on a previously published lithographic process including e-beam evaporation of 150 nm of Au on a 10-nm Ti adhesion layer [25], a tailor-made 12-channel bipotentiostat with miniaturised PCB and data acquisition software [26]. In addition to the array of 12 IDEs, each of the independently addressable measurement sites of the microelectrode chip contains a large counter and a reference electrode that have been used in other cell-based applications [4, 27].

As schematically presented by Caviglia et al. 2015 [18], two 5-mm thick micromilled poly(methyl methacrylate) (PMMA) layers are assembled on top of each other. The lower layer is used as a holder for the microelectrode chip, while the upper layer, having an opening in the middle, defines a 600 µl-well for cell culturing. A polydimethylsiloxane (PDMS) gasket is placed between the microelectrode chip and the upper PMMA layer to form a liquid-tight sealing of the vial. Each of the two combs of the IDEs (WEa and WEb)

is independently addressable and composed of 12 digits (length 500 μm; width and gap 10 μm).

EIS monitoring protocol

EIS recordings were programmed to enable continuously monitoring at the time interval of 1 h over the entire experimental period. Measurement was performed in regular culture medium (DMEM supplemented with 10% FBS and 1% P/S). The applied sinusoidal perturbation potential was set to 200 μV. Full spectra were acquired measuring 30 points in the frequency range from 100 Hz to 100 kHz. One hundred kilohertz was found to be the frequency corresponding to the most sensitive region of the spectrum, as previously shown with Bode plots [18]. To achieve a satisfactory noise reduction, each point of the spectrum was measured with an average time of 2 s. The impedance measurements were performed using the coplanar sensing configuration (WEa vs. WEb), previously shown to provide the best sensitivity [28].

Cytotoxicity assays

For EIS monitoring of drug-induced cytotoxicity, three different HT1080 cell densities (2.5×10^4, 7.5×10^4, 1×10^5 cells/cm^2) were seeded on laminin-modified microelectrode chips. Ten hours after cell seeding, free OxPt in PBS was added to the cell culture well to obtain final concentrations of 25, 50, 100 and 200 μM. To compare the cytotoxicity induced by free OxPt with that of OxPt-loaded liposomes, the same experiment was performed using 100 μM solutions (in 0.1% NaCl) of PEG-Lipo-OxPt, De-PEG-Lipo-OxPt and Stealth liposomes. Control experiments were performed by adding 0.1% NaCl to the cell culture well in the absence of OxPt.

Cell viability was measured and quantified by the standard colorimetric MTS assay in 96-well plates. The MTS assay is an end-point assay that measures changes in the mitochondrial metabolism of the cells [10]. The used cell densities were the same as described for EIS monitoring. Ten hours after seeding, the cells were treated and incubated with 3.125, 6.25, 12.5, 25, 50, 100 and 200 μM of OxPt. After 24, 48 and 72 h, 20 μl of MTS solution was added, followed by an additional incubation for 1 h at 37 °C, and absorbance measurement at 490 nm. Control experiments were performed under the same conditions as used for EIS monitoring. The measured absorbance for each incubated cell population was normalised with respect to the absorbance of the control.

EIS data analysis and statistics

Changes in impedance were expressed using the dimensionless parameter Cell Index (CI) [12, 18], which represents the maximum value of the normalised impedance, Eq. 1

$$Cell\ index(t) = max_{i=1,\ldots,n} \frac{|Z(t,f_i)| - |Z(0,f_i)|}{|Z(0,f_i)|} \quad (1)$$

where $|Z(t,f_i)|$ is the magnitude of the impedance at a given frequency and time point and $|Z(0,f_i)|$ is the magnitude of the impedance at the same frequency at the beginning of the experiment recorded in the absence of cells. In this work, for each time point, the CI was calculated analysing the complete spectrum ($N = 30$). MatLab (R2013a) was used to create specific algorithms for data processing and analysis.

To quantify the time dependence of cell death, the half maximal inhibitory time (IT50) was calculated as defined by [17]. IT50 is analogous to the half maximal inhibitory concentration (IC50), as a quantitative measure to indicate how much time is required for the drug to cause 50% decrease in cell viability. The sigmoidal fitting of the data and the IT50 values were calculated using the logistic 4-parameter function (Origin (version 9.0)).

For each experiment, the acquired EIS data on the microelectrode arrays were processed and averaged. Each experiment was repeated at least twice using a minimum of 12 and a maximum of 18 interdigitated electrodes $n = 12$ or 18. Data are presented as average ± standard deviation.

Real-time BF imaging

Real-time BF imaging was performed to support the EIS data by following the same protocol. HT1080 were seeded at the density of 7.5×10^4 cells/cm^2 on laminin-modified transparent 96-well plates. BF imaging was performed using the oCelloScope microscope scanning system (Philips BioCell A/S, Allerød, Denmark), located in a standard cell culture incubator and maintained at 37 °C. Images were acquired every 20 min for the first 6 h and every 2 h over the last 64 h. Three independent experiments were performed in quadruplicate and cells were monitored for changes in morphology. The percentage of covered area was extracted from raw images using a dedicated MatLab script by Philips BioCell A/S.

Results

Chemotherapy represents one of the most commonly used therapeutic strategies for treating cancer [29–31]. TDDSs have been developed to increase the efficacy of treatment by specifically targeting the tumour, thereby reducing side effects of the administered drugs [32]. With the help of TDDSs, anticancer drugs can be directed to the tumour site, resulting in locally increased drug concentration and/or decreased exposure of healthy tissue [33]. During the past 40 years, liposomal TDDS have been in the spotlight for anticancer drug development [34, 35]. Although most liposome-based TDDS

strategies employ PEG to obtain stable and long circulating formulations [36], this modification has shown to reduce cellular endocytosis and release of the cargo [37]. Both intrinsic and extrinsic stimulation strategies have been pursued to ensure a specific drug release trigger at the tumour site, following more efficient endocytosis. Intrinsic stimulation strategies exploit biochemical differences between healthy and cancer cells, such as pH [38] and local expression of tumour-specific enzymes [39], while extrinsic stimulation strategies involve temperature-, light- and magnetic field–induced release [40]. MMPs are overexpressed in a wide range of tumours; therefore, these specific enzymes have been used in the development of tumour-specific drug delivery systems [41]. In fact, this group of extracellularly secreted enzymes is known to be involved in several processes of cancer development, including angiogenesis, invasion and metastasis, as they take part in the proteolysis of the extracellular matrix proteins and basement membranes [42]. Therefore, the ability of MMPs to degrade peptides and proteins is exploited to trigger and control the liposomal drug release at the tumour site by using ad hoc engineered liposome carriers [43]. Liposomes can be functionalised with a lipid anchor coupled to a peptide (lipopeptide), containing an MMP cleavage site, which is cleaved by overexpressed MMPs in the tumour. The MMPs can also cleave off PEG-modified peptides present on the surface of the liposome membrane, leading to de-PEGylation and electrostatic attraction of the subsequently positively charged liposomes to the cancer cell surface and subsequent internalisation (Fig. 1) [43].

Optimisation of cell seeding density

To ensure reliable EIS-based cytotoxicity assays, the initial cell density must be optimised. As previously described [17], the optimal seeding density must provide control growth curves characterised by a stable steady state for the entire duration of the experiment. Different densities (2.5×10^4, 7.5×10^4, 1×10^5 cells/cm^2) of HT1080 cells were seeded and their proliferation was continuously monitored over 70 h. Figure 2 a shows the CI profiles over 70 h related to the adhesion and proliferation of HT1080 cells. Both 7.5×10^4 and 1×10^5 cells/cm^2 provide a steadily increasing CI profile until reaching a plateau (CI = 1.1 and 1.3) 60 and 50 h after seeding, respectively. Reaching a plateau reflects the establishment of a confluent cell layer on the microelectrode array surfaces. For the lower cell density (2.5×10^4 cells/cm^2), a 20 h lag phase is observed, followed by a slow but steady increase in CI. Although all tested cell densities could in principle be used for cytotoxicity experiments, higher cell seeding densities provide better signal-to-noise ratio and, after reaching a steady state, proliferation can be monitored for a sufficiently long period to facilitate a reliable performance of the assay. A cell density of 7.5×10^4 was chosen for all subsequent experiments to obtain approximately 20% cell coverage 24 h after seeding. This results in a growth curve characterised by a stable steady state as well as good signal-to-noise ratio.

Cytotoxicity of free OxPt

OxPt is a third-generation platinum-based anticancer drug [44] which has shown potency against a wide range of cancer cells, both in vitro and in vivo [45]. In clinical applications, it is used as a chemotherapeutic agent for the treatment of metastatic colorectal carcinoma in combination with fluoropyrimidines [46]. Among the several mechanisms of action that have been proposed for OxPt, the main accepted one is related to DNA intercalation and damage, resulting in cell growth inhibition and apoptosis [47]. The cytotoxic effect of different concentrations of free OxPt on HT1080 cells was first evaluated using the MTS end-point assay, which reflects decrease in the mitochondrial metabolism [10]. Based on the linear portion of the plotted MTS assay results (Fig. 2b), final OxPt concentrations of 0 (control), 25, 50, 100 and 200 μM were chosen for the EIS assay (Fig. 2c). Cells were seeded on the microelectrode arrays with an initial density of 7.5×10^4 cells/cm^2. Ten hours after cell seeding, OxPt was added to the cell media to achieve above-mentioned final concentrations. Figure 2 c shows the real-time cytotoxicity response of HT1080 cells to the different OxPt concentrations (presented as relative CI where 100% indicates the value for each population before introduction of OxPt). As seen, the control experiment shows a steady CI profile for the entire duration of the experiment. The cytotoxic response is, as expected, faster with increasing OxPt concentrations (Fig. 2c). The CI profiles related to 25, 50, 100 and 200 μM OxPt show an initial increase, which after 10, 20 and 30 h, respectively, is followed by a subsequent decrease towards 0. In our previous studies, performed using the same microelectrode array chip under both static and perfusion conditions [17], the same increase in CI behaviour was observed and found to be due to an intensified cellular metabolic activity [48, 49] as well as changes in cell morphology and adhesion properties in response to stress induced by accumulation of the drug before onset of cell death [17, 50]. To quantify and compare the cytotoxic effect of different OxPt concentrations, the IT50 values (Fig. 2d) were calculated for each condition, based on the data presented in Fig. 2c, showing a clear decrease in IT50 with increasing OxPt concentration.

Cytotoxicity of OxPt-loaded liposomes

The cytotoxic effect of OxPt-containing MMP-sensitive PEGylated liposomes (PEG-Lipo-OxPt) was assayed and compared with free OxPt. Although, HT1080 cells overexpress MMPs both in vitro and in vivo [43], to mimic the

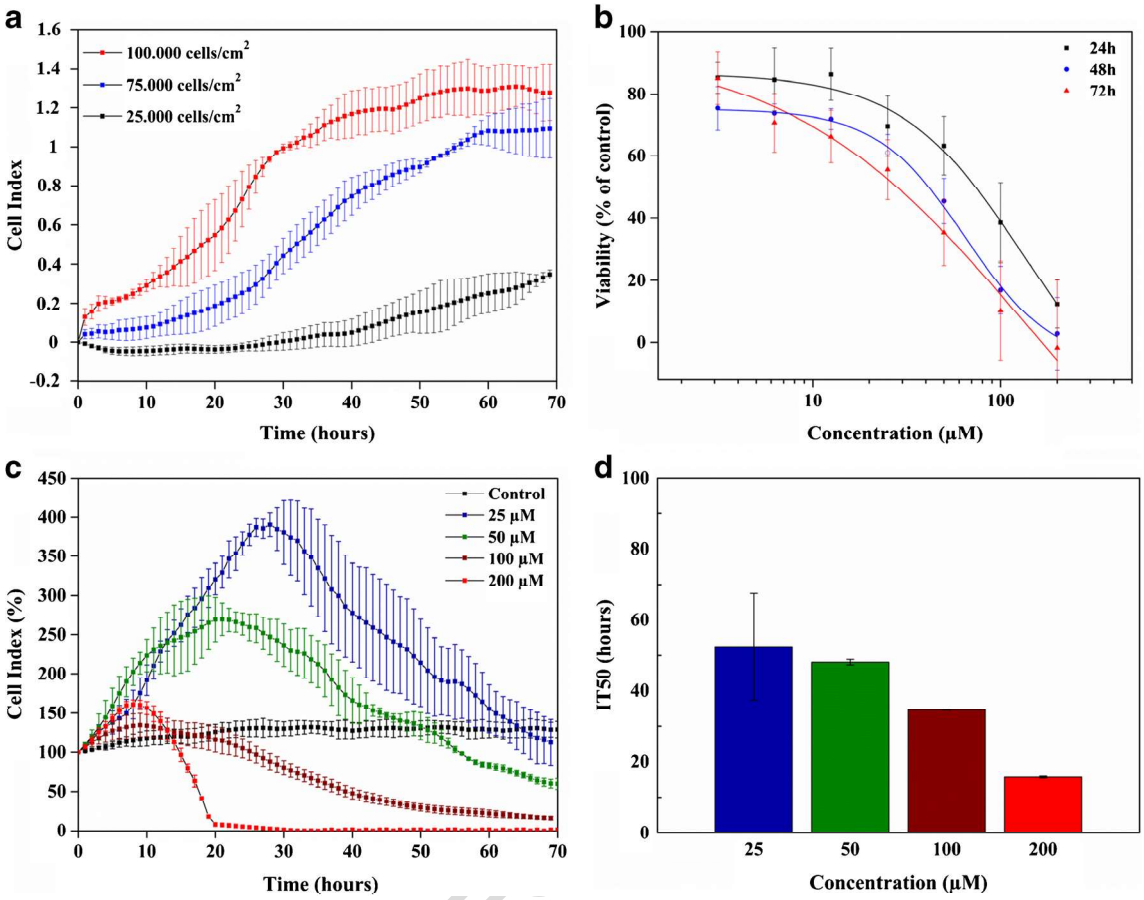

Q2 **Fig. 2** Evaluation of cytotoxicity of free OxPt on the HT1080 cell line using real-time EIS and end-point MTS assay. **a** Optimisation of cell seeding density for EIS measurements. **b** MTS assay evaluating cell viability at different concentrations of free OxPt at different end-points. **c** Real-time EIS assay evaluating cell viability at different concentrations of free OxPt. **d** Half maximal inhibitory time (IT50) extracted from **c** for the different concentrations of free OxPt. For **b**–**d**, the cell seeding density was always 7.5×10^4 cells/cm^2. Standard deviation where calculated based on $n = 12$–18 (**a**, **c** and **d**) and $n = 3$ (**b**)

cleavage by MMPs, de-PEGylation of the PEG-Lipo-OxPt with the protease thermolysin was also performed, generating De-PEG-Lipo-OxPt, which was used as a de-PEGylation control for the cytotoxicity assay. De-PEGylation by MMPs or thermolysin leads to the generation of cationic liposomes, electrostatic attraction of the positively charged liposomes to the cancer cell surface and subsequent internalisation (Fig. 1) [43].

To perform real-time EIS assays, HT1080 cells were seeded on the microelectrode arrays with the same initial density of 7.5×10^4 cells/cm^2 as above. Ten hours after cell seeding, the different compounds (free OxPt, PEG-Lipo-OxPt, De-PEG-Lipo-OxPt) were added to the cell media to achieve a final concentration of 100 µM OxPt. A control experiment was performed in drug-free medium. Figure 3 a shows the cytotoxic response of HT1080 cells to the different OxPt-containing liposome formulations compared with the effect of free OxPt. The control (without drug) shows a stable CI profile after reaching confluence. When the cells were exposed to PEG-Lipo-OxPt, the impedance profile showed a negative CI peak down to 80% during the first 5 h after drug addition, followed by a continuous increase until the onset of the cytotoxicity at a CI of 140%, 25 h after addition of the drug. Likewise, De-PEG-Lipo-OxPt induces a similar but more pronounced response with a negative CI peak in the first 5 h after drug addition, down to 50% which increases up to 200% until the start of cytotoxicity at 25 h after addition of the drug. Compared with free OxPt, the cytotoxic effect of the liposome formulations (PEG-Lipo-OxPt and De-PEG-Lipo-OxPt) is slower. However, both formulations lead to (i) a decrease in CI in the initial 5 h, (ii) a dramatic CI increase up to 26 h post drug addiction and (iii) onset of cytotoxicity and cell death 70 h after drug treatment.

The behaviour of PEG-Lipo-OxPt and De-PEG-Lipo-OxPt compared with free OxPt is expected and can be explained by a slower release of the drug when contained in a liposome formulation. The cytotoxicity of free OxPt is faster with cell death appearing already 10 h after drug addition, when a slow decrease in CI towards 0 takes place. The slower effect of PEG-Lipo-OxPt compared to De-PEG-Lipo-OxPt is likely

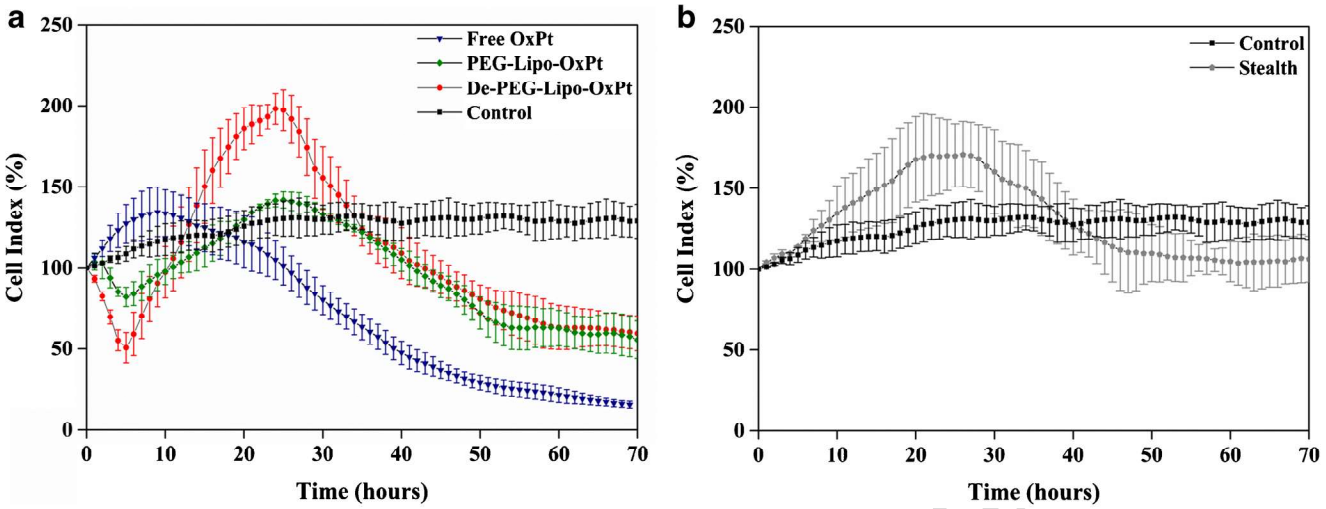

Fig. 3 Real-time EIS monitoring of the effect of different formulation of OxPt on HT1080 cells. **a** Signal recorded when cells where incubated with free OxPt, PEG-Lipo-OxPt and De-PEG-Lipo-OxPt. **b** Signal recorded in presence of OxPt-loaded Stealth compared with the signal in absence of the drug (control). Standard deviation where calculated based on $n = 12$ or 18

due to the low MMP expression of HT1080 cells in vitro and as consequence an incomplete cleavage of the PEGylated peptides, thus reduced uptake and degradation of the liposomes. Figure 3 b shows the CI profile recorded after exposure of cells to OxPt-loaded Stealth liposomes. These liposomes are not sensitive to extracellular MMPs and cannot be degraded and should thus not have any cytotoxic effect. An initial large CI increase is however seen followed by a stabilisation around a CI of 100%. Previously, it was found that Stealth do have a low toxicity, suggesting a low spontaneous drug leakage (unpublished work), and low cell toxicity which is in good agreement with our finding (Fig. 3b).

The initial negative CI peak obtained from PEG-Lipo-OxPt and De-PEG-Lipo-OxPt was not observed for free OxPt or Stealth and can be due to different mechanisms of cell endocytosis for liposomes [51] compared with free drugs. The more pronounced initial negative CI peak for De-PEG-Lipo-OxPt suggests more effective endocytosis of these liposomes, due to the direct exposure of cells to cationic lipids.

In order to further interpret and understand the EIS data, we used real-time BF imaging as a comparison. The HT1080 cells were seeded at 7.5×10^4 cells/cm^2 on laminin-modified transparent 96-well plates (the same conditions and density as on the microelectrode array). The cell growth and the effect of liposomal formulations were monitored for 70 h.

The morphological changes in the HT1080 cells, induced by free and OxPt-loaded liposomes, were recorded with real-time BF imaging and compared with real-time EIS data, as shown in Fig. 4 (see also Electronic Supplementary Material videos V1_Control, V2_FreeOxPt, V3_PEG-Lipo-OxPt, V4_De-PEG-Lipo-OxPt and V5_Stealth). When evaluating BF images recorded from cells exposed to free OxPt (Fig. 4F–H), no morphological changes are observed. The cell death shown in Fig. 4I–J correlates well with the EIS data with a CI approaching 0 at 70 h. It should be noticed that for the control, the CI was stable and cells alive, covering the bottom of the cell culture plate after 70 h (Fig. 4A–E).

Endocytosis has previously been described as a result of morphological changes of the plasma membrane [52], which leads to a temporary decrease in cell adhesion. As can be seen in Fig. 4L and Q, when cells are exposed to PEG-Lipo-OxPt and De-PEG-Lipo-OxPt, they tend to round up and hence decrease their adhesion to the surface. For both formulations, the rounding up of cells after 5 h correlates well with the initial abrupt dip in the CI measured with EIS at the same time point. Subsequent re-adhesion of cells can be observed after 10 h (Fig. 4M and R), which also can be followed by EIS as a continuous increase in the CI until about 26 h, when cell death sets in. From the BF images (Fig. 4N and S), no significant difference can be seen in cell morphology upon treatment with PEG-Lipo-OxPt and De-PEG-Lipo-OxPt. On the other hand, this can clearly be distinguished using EIS. As previously presented, the increase in CI is attributed to intensified cellular metabolic activity [48, 49] as well as changes in cell morphology and adhesion properties in response to stress before onset of cell death [17, 50]. When assessing the effect of the Stealth, BF images (Fig. 4U–X) do not show any significant difference in comparison with the control (Fig. 4A–D). However, EIS measurements show an increase in CI until 26 h, followed by a return to the initial CI. The observed increased in CI cannot be readily explained, since the Stealth formulation should not be taken up by the cells. The return of the CI to the initial level indicates that Stealth only has a marginal toxic effect, which also can be seen in Fig. 4Y.

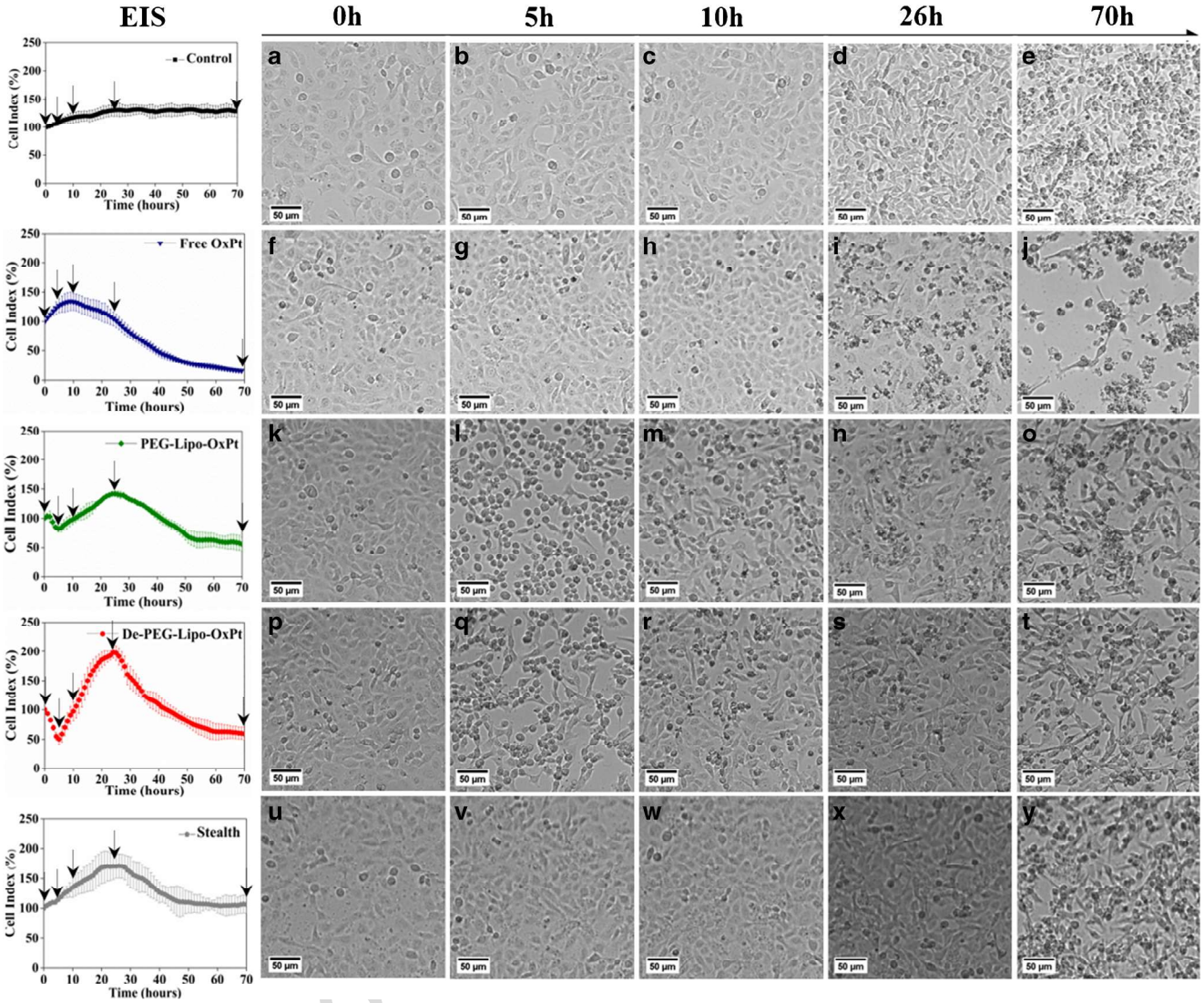

Q3 **Fig. 4** Representative real-time BF images (right) and EIS data (left, from Fig. 3) of HT1080 cells recorded under the same conditions in the absence (control) and presence of free OxPt and when exposed to different liposomal formulations: PEG-Lipo-OxPt, De-PEG-Lipo-OxPt and OxPt-loaded Stealth. The arrows in the EIS figures indicate 0, 5, 10, 26 and 70 h. All scale bars in A–Y are 50 µm

The relative surface coverage was calculated after 5 and 12 h, for BF images using the MatLab script (Philips BioCell A/S), and for EIS data from the relative decrease in CI, for PEG-Lipo-OxPt and De-PEG-Lipo-OxPt (Fig. 5). Based on the information gathered from BF images, the effect of the two liposomal formulations cannot be distinguished; however, when looking at the EIS data, we observe a significant difference between PEG-Lipo-OxPt and De-PEG-Lipo-OxPt, which clearly shows that EIS is more sensitive to cell morphological changes than BF imaging.

Conclusions

Our findings show the benefit of using real-time detection methods such as EIS for evaluating cytotoxic effects and the ability to record endocytosis events in cells. Real-time BF imaging was used to visualize cell morphological changes in order to explain the EIS results, especially during the first 5 h when a short-term decrease in CI was observed representing endocytotic events. The BF images clearly show a rounding up of cells, detachment and a subsequent drastic decrease in the cell coverage during these first 5 h for OxPt-loaded liposomes (except for Stealth), which is a hallmark of liposome endocytosis. This overall EIS response can be divided into three different stages: (i) a decrease in CI within the first 5 h, i.e. the same time point for which BF images show rounding up and detachment of cells, demonstrating the capability of EIS to record liposome endocytosis; (ii) reattachment of cells and a subsequent increase in CI until onset of cytotoxicity; and (iii) decrease in CI due to continued cytotoxicity. This behaviour was not observed when using free OxPt or OxPt-loaded

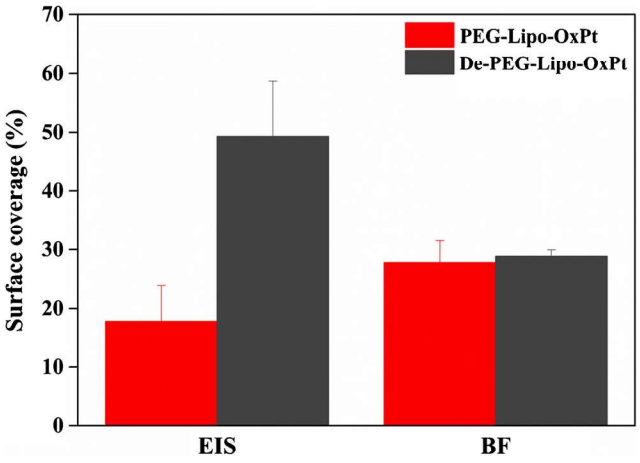

Fig. 5 Comparison of relative decrease in surface area coverage (%) between EIS and BF data after 5 and 12 h, for OxPt-loaded PEGgylated (PEG-Lipo-OxPt) and de-PEGylated (De-PEG-Lipo-OxPt) liposomes. Relative surface coverage was calculated from MatLab script for BF images, and from CI for EIS data

Stealth liposomes, which do not undergo endocytosis. When comparing the events recorded for PEG-Lipo-OxPt and De-PEG-Lipo-OxPt, EIS was shown to be more sensitive to the changes in cell morphology induced by liposome endocytosis than BF imaging.

Acknowledgements We acknowledge Rasmus Eliasen for the help with liposomes de-PEGylation.

Funding information The authors received funding from the EU for the FP7 project EXCELL (NMP4-SL-2008-214706) and the Horizon 2020 MSCA-ITN project Training4CRM (H2020-MSCA-ITN-2016). Kinga Zór received the financial support during the preparation of the manuscript from the Danish National Research Foundation (DNRF122) and Villum Fonden (Grant No. 9301) for Intelligent Drug Delivery and Sensing Using Microcontainer and Nanomechanics (IDUN).

Compliance with ethical standards

Conflict of interest The authors declare that there are no conflicts of interest.

Human participants and/or animals The studies presented in this article comprise neither human participants nor animals.

References

1. Liu Q, Yu J, Xiao L, Cheuk J, Tang O, Zhang Y, et al. Impedance studies of bio-behavior and chemosensitivity of cancer cells by micro-electrode arrays. Biosens Bioelectron. 2009;24:1305–10. https://doi.org/10.1016/j.bios.2008.07.044.
2. Minchinton AI, Tannock IF. Drug penetration in solid tumours. Nat Rev Cancer. 2006;6:583–92. https://doi.org/10.1038/nrc1893.
3. Kepp O, Galluzzi L, Lipinski M, Yuan J, Kroemer G. Cell death assays for drug discovery. Nat Rev Drug Discov. 2011;10:221–37. https://doi.org/10.1038/nrd3373.
4. Zór K, Heiskanen A, Caviglia C, Vergani M, Landini E, Shah F, et al. A compact multifunctional microfluidic platform for exploring cellular dynamics in real-time using electrochemical detection. RSC Adv. 2014;4:63761–71. https://doi.org/10.1039/c4ra12632g.
5. Garvey CM, Spiller E, Lindsay D, Chiang C-T, Choi NC, Agus DB, et al. A high-content image-based method for quantitatively studying context-dependent cell population dynamics OPEN. Nat Publ Gr. 2016. https://doi.org/10.1038/srep29752.
6. Radmacher M. Studying the mechanics of cellular processes by atomic force microscopy. Methods Cell Biol. 2007;83:347–72. https://doi.org/10.1016/S0091-679X(07)83015-9.
7. Spiller DG, Wood CD, Rand DA, White MRH. Measurement of single-cell dynamics INSIGHT REVIEW. Nature. 2010;465:736–45. https://doi.org/10.1038/nature09232.
8. Wakefield ID, Pollard C, Redfern WS, Hammond TG, Valentin J-P. The application of in vitro methods to safety pharmacology. Fundam Clin Pharmacol. 2002;16:209–18.
9. Rampersad SN, Rampersad NS. Multiple applications of Alamar Blue as an indicator of metabolic function and cellular health in cell viability bioassays. Sensors. 2012;12:12347–60. https://doi.org/10.3390/s120912347.
10. Malich G, Markovic B, Winder C (1997) The sensitivity and specificity of the MTS tetrazolium assay for detecting the in vitro cytotoxicity of 20 chemicals using human cell lines.
11. Fang Y (2006) Label-free cell-based assays with optical biosensors in drug discovery.
12. Xi B, Yu N, Wang X, Xu X, Abassi Y. The application of cell-based label-free technology in drug discovery. Biotechnol J. 2008;3:484–95. https://doi.org/10.1002/biot.200800020.
13. Patching SG. Surface plasmon resonance spectroscopy for characterisation of membrane protein-ligand interactions and its potential for drug discovery. BBA - Biomembr. 2014;1838:43–55. https://doi.org/10.1016/j.bbamem.2013.04.028.
14. Giaever I, Keese CR. Monitoring fibroblast behavior in tissue culture with an applied electric field. Proc Natl Acad Sci U S A. 1984;81:3761–4. https://doi.org/10.1073/pnas.81.12.3761.
15. Wegener J, Keese CR, Giaever I. Electric cell-substrate impedance sensing (ECIS) as a noninvasive means to monitor the kinetics of cell spreading to artificial surfaces. Exp Cell Res. 2000;259:158–66. https://doi.org/10.1006/excr.2000.4919.
16. Giaever I, Keese CR (1991) Micromotion of mammalian cells measured electrically (cell motility/fibroblast behavior/nanometer motions/electrical measurements).
17. Caviglia C, Zór KZ, Montini L, Tilli V, Canepa S, Melander F, et al. Impedimetric toxicity assay in microfluidics using free and liposome-encapsulated anticancer drugs. Anal Chem. 2015;87:2204–12. https://doi.org/10.1021/ac503621d.
18. Caviglia C, Zór K, Canepa S, Carminati M, Larsen LB, Raiteri R, et al. Interdependence of initial cell density, drug concentration and exposure time revealed by real-time impedance spectroscopic cytotoxicity assay. Analyst. 2015;140:3623. https://doi.org/10.1039/c5an00097a.
19. Ceriotti L, Ponti J, Broggi F, Kob A, Drechsler S, Thedinga E, et al. Real-time assessment of cytotoxicity by impedance measurement on a 96-well plate. Sensors Actuators B. 2007;123:769–78. https://doi.org/10.1016/j.snb.2006.10.024.
20. Lundstrom K. Cell-impedance-based label-free technology for the identification of new drugs. Expert Opin Drug Discov. 2017;12:335–43. https://doi.org/10.1080/17460441.2017.1297419.
21. Starkuviene V, Pepperkok R. The potential of high-content high-throughput microscopy in drug discovery. Br J Pharmacol. 2007;152:62–71. https://doi.org/10.1038/sj.bjp.0707346.
22. Liu Z, Lavis LD, Betzig E. Imaging live-cell dynamics and structure at the single-molecule level. Mol Cell. 2015;58:644–59. https://doi.org/10.1016/j.molcel.2015.02.033.
23. Isherwood B, Timpson P, McGhee EJ, Anderson KI, Canel M, Serrels A, et al. Live cell in vitro and in vivo imaging applications:

accelerating drug discovery. Pharmaceutics. 2011;3:141–70. https://doi.org/10.3390/pharmaceutics3020141.
24. Fischer LM, Tenje M, Heiskanen AR, Masuda N, Castillo J, Bentien A, et al. Gold cleaning methods for electrochemical detection applications. Microelectron Eng. 2008;86(86):1282–5. https://doi.org/10.1016/j.mee.2008.11.045.
25. Dimaki M, Vergani M, Heiskanen A, Kwasny D, Sasso L, Carminati M, et al. A compact microelectrode array chip with multiple measuring sites for electrochemical applications. Sensors. 2014;14:9505–21. https://doi.org/10.3390/s140609505.
26. Vergani M, Carminati M, Ferrari G, Landini E, Caviglia C, Heiskanen A, et al. Multichannel bipotentiostat integrated with a microfluidic platform for electrochemical real-time monitoring of cell cultures. IEEE Trans Biomed Circuits Syst. 2012;6:498–507. https://doi.org/10.1109/TBCAS.2012.2187783.
27. Sasso L, Heiskanen A, Diazzi F, Dimaki M, Le'on JC, Vergani M, et al. Doped overoxidized polypyrrole microelectrodes as sensors for the detection of dopamine released from cell populations. Analyst. 2013;138:3651–9. https://doi.org/10.1039/c3an00085k.
28. Caviglia C, Carminati M, Heiskanen A, Vergani M, Ferrari G, Sampietro M, et al. Quantitative label-free cell proliferation tracking with a versatile electrochemical impedance detection platform. J Phys Conf Ser. 2012;407:012029. https://doi.org/10.1088/1742-6596/407/1/012029.
29. Hoelder S, Clarke PA, Workman P. Discovery of small molecule cancer drugs: successes, challenges and opportunities. Mol Oncol. 2012;6:155–76. https://doi.org/10.1016/j.molonc.2012.02.004.
30. Hengel SR, Spies MA, Spies M. Small-molecule inhibitors targeting DNA repair and DNA repair deficiency in research and cancer therapy. Cell Chem Biol. 2017;24:1101–19. https://doi.org/10.1016/j.chembiol.2017.08.027.
31. Belizário JE, Sangiuliano BA, Perez-Sosa M, Neyra JM, Moreira DF. Using pharmacogenomic databases for discovering patient-target genes and small molecule candidates to cancer therapy. Front Pharmacol. 2016;7:312. https://doi.org/10.3389/fphar.2016.00312.
32. Rani K, Paliwal S. A review on targeted drug delivery: its entire focus on advanced therapeutics and diagnostics. Sch J Appl Med Sci. 2014;2:328–31. https://doi.org/10.1016/j.biopha.2004.01.007.
33. Mishra N, Pant P, Jaiswal J. Targeted drug delivery : a review targeted drug delivery : a review. Am J PharmTechnol Res. 2016;6:1–24.
34. Sharma G, Anabousi S, Ehrhardt C, Kumar MNVR. Liposomes as targeted drug delivery systems in the treatment of breast cancer. J Drug Target. 2006;14:301–10. https://doi.org/10.1080/10611860600809112.
35. Samad A, Sultana Y, Aqil M. Liposomal drug delivery systems: an update review. Curr Drug Deliv. 2007;4:297–305. https://doi.org/10.2174/156720107782151269.
36. Sercombe L, Veerati T, Moheimani F, Wu SY, Sood AK, Hua S. Advances and challenges of liposome assisted drug delivery. Front Pharmacol. 2015;6:286. https://doi.org/10.3389/fphar.2015.00286.
37. Verhoef JJF, Anchordoquy TJ. Questioning the use of PEGylation for drug delivery. Drug Deliv Transl Res. 2013;3:499–503. https://doi.org/10.1007/s13346-013-0176-5.
38. Paliwal SR, Paliwal R, Vyas SP. Drug delivery a review of mechanistic insight and application of pH-sensitive liposomes in drug delivery a review of mechanistic insight and application of pH-sensitive liposomes in drug delivery. Drug Deliv. 2015;22:231–42. https://doi.org/10.3109/10717544.2014.882469.
39. Fouladi F, Steffen KJ, Mallik S. Enzyme-responsive liposomes for the delivery of anticancer drugs. Bioconjug Chem. 2017;28:857–68. https://doi.org/10.1021/acs.bioconjchem.6b00736.
40. Deshpande PP, Biswas S, Torchilin VP. Current trends in the use of liposomes for tumor targeting. Nanomedicine (Lond). 2013;8:1509–28. https://doi.org/10.2217/nnm.13.118.
41. Gialeli C, Theocharis AD, Karamanos NK. Roles of matrix metalloproteinases in cancer progression and their pharmacological targeting. FEBS J. 2011;278:16–27. https://doi.org/10.1111/J.1742-4658.2010.07919.X.
42. Jabłońska-Trypuć A, Matejczyk M, Rosochacki S, Jabłon AJ, Trypuć J-T. Matrix metalloproteinases (MMPs), the main extracellular matrix (ECM) enzymes in collagen degradation, as a target for anticancer drugs Matrix metalloproteinases (MMPs), the main extracellular matrix (ECM) enzymes in collagen degradation, as a target for anticancer drugs. J Enzym Inhib Med Chem. 2016;31:177–83. https://doi.org/10.3109/14756366.2016.1161620.
43. Gjetting T, Jølck RI, Andresen TL. Effective nanoparticle-based gene delivery by a protease triggered charge switch. Adv Healthc Mater. 2014;3:1107–18. https://doi.org/10.1002/adhm.201300503.
44. Kelland L. The resurgence of platinum-based cancer chemotherapy. Nat Rev Cancer. 2007;7:573–84. https://doi.org/10.1038/nrc2167.
45. Raymond E, Faivre S, Woynarowski JM, Chaney SG. Oxaliplatin: mechanism of action and antineoplastic activity. Semin Oncol. 1998;25:4–12.
46. Adams RA, Meade AM, Seymour MT, Wilson RH, Madi A, Fisher D, et al. Intermittent versus continuous oxaliplatin and fluoropyrimidine combination chemotherapy for first-line treatment of advanced colorectal cancer: results of the randomised phase 3 MRC COIN trial. Lancet Oncol. 2011;12:642–53. https://doi.org/10.1016/S1470.
47. Alcindor T, Beauger N. Oxaliplatin: a review in the era of molecularly targeted therapy. Curr Oncol. 2011;18:18–25. https://doi.org/10.3747/co.v18i1.708.
48. Seeland S, Kettiger H, Murphy M, Treiber A, Giller J, Kiss A, et al. ATP-induced cellular stress and mitochondrial toxicity in cells expressing purinergic P2X7 receptor. Pharmacol Res Perspect. 2015;3:1–13. https://doi.org/10.1002/prp2.123.
49. Meissner R, Eker B, Kasi H, Bertsch A, Renaud P. Distinguishing drug-induced minor morphological changes from major cellular damage via label-free impedimetric toxicity screening. Lab Chip. 2011;11:2352–61. https://doi.org/10.1039/c1lc20212j.
50. Kobayashil H, Takemura Y, Ohnuma T. Relationship between tumor cell density and drug concentration and the cytotoxic effects of doxorubicin or vincristine: mechanism of inoculum effects*. Cancer Chemother Pharmacolcer Chemother Pharmacol. 1992;31:6–10.
51. Straubinger RM, Hong K. Endocytosis of liposomes and intracellular fate of encapsulated molecules : encounter with a low pH compartment after internalization in coated vesicles. 1983;32:1069–79.
52. Yoshida A, Sakai N, Uekusa Y, Imaoka Y, Itagaki Y, Suzuki Y, et al. Morphological changes of plasma membrane and protein assembly during clathrin-mediated endocytosis. PLoS Biol. 2018:16. https://doi.org/10.1371/journal.pbio.2004786.

AUTHOR QUERIES

AUTHOR PLEASE ANSWER ALL QUERIES.

Q1. Please check if the affiliations are presented correctly.
Q2. Please check if the figure captions are presented correctly.
Q3. Figure 4 and Graphical Abstract contains poor quality and small text inside the artwork. Please do not re-use the file that we have rejected or attempt to increase its resolution and re-save. It is originally poor, therefore, increasing the resolution will not solve the quality problem. We suggest that you provide us the original format. We prefer replacement figures containing vector/editable objects rather than embedded images. Preferred file formats are eps, ai, tiff and pdf.
Q4. Please check if the "Acknowledgements" and the "Funding information" statements are presented correctly.
Q5. Please supply/verify the standard abbreviation of the journal name in References [32, 50].
Q6. Please provide complete bibliographic details of this references [10, 11, 16, 51].